CrystEngComm

PAPER

View Article Online
View Journal | View Issue



Cite this: *CrystEngComm*, 2024, **26**, 5469

# Synthesis of a hierarchical TS-1 zeolite with tunable macropore size and its performance in the catalytic oxidation reactions†

Shengjie Zhu,[ab] Xiaomin Zhang,*[a] Lei Dong,[ab] Yangyang Yuan,[a] Xiuyun Ma,[a] Yanping Chen [a] and Lei Xu *[a]

Received 16th July 2024,
Accepted 28th August 2024

DOI: 10.1039/d4ce00706a

rsc.li/crystengcomm

Hierarchically structured materials are considered to be one of the important options to enhance the mass transportation efficiency in microporous zeolites. Herein, we reported a highly efficient steam-assisted crystallization strategy for the synthesis of a hierarchical TS-1 zeolite with a tunable macropore size. The amorphous $SiO_2$–$TiO_2$ precursor dissolved gradually and acted as both a nutrient supplier and macropore template *in situ*. The framework Ti content of the synthesized TS-1 zeolites could be tuned over a wide range (Ti wt% = 0.70–1.39) by varying the Ti content of the $SiO_2$–$TiO_2$ precursor. Moreover, the pore size of the macropores could be modulated according to the particle size of the precursor based on the investigation of the formation mechanism of the macropores in the hierarchical TS-1 zeolite. The hierarchical TS-1 zeolite exhibited better catalytic activity in the epoxidation reaction of 1-hexene and hydroxylation of phenol compared to the typical microporous zeolites. The improved performance of the hierarchical TS-1 zeolite was probably caused by the improved diffusion performance of the hierarchical structure.



## Introduction

Zeolites have been widely used in the field of catalysis, ion-exchange, and adsorption/separation due to their unique pore structure, high hydrothermal stability, and rich surface acid–base properties. Among the various zeolites, titanium silicalite-1 (TS-1) zeolite in which there is the isomorphous substitution of Si by Ti in the silicalite-1 frameworks was first synthesized by Taramasso *et al.* in 1983.[1] Due to its MFI-type topology and active titanium centres, TS-1 zeolite shows excellent activity and high selectivity under mild reaction conditions in the reaction system using $H_2O_2$ as an oxidant. TS-1 zeolite has been proven to be one of the most efficient catalysts in a number of selective oxidation reactions such as olefin epoxidation,[2,3] aromatic hydroxylation,[4,5] ketone ammoximation[6,7] and oxidative desulfurization.[8,9]

However, as a typical MFI-type zeolite, its inherent microporous channels of about 0.55 nm lead to diffusion limitations to the internal active sites, resulting in severe mass transfer resistance of the reactants and products in some reactions especially when bulky molecules are involved.[10,11] Reducing the size of zeolite to prepare nanocrystals is one of the ways to alleviate the diffusion limitations. Nanocrystals show higher catalytic activities than conventional zeolites because of less diffusion limitations of reactants and products as well as more active sites in the small crystals. However, the yield of the nanocrystals was low and a large number of microporous structure-directing agents in the hydrothermal synthesis system were usually required. Moreover, it is difficult to filter and recycle when the nanocrystals are used in the industrial process due to their small size.[12,13]

The introduction of mesopores/macropores, in addition to the intrinsic microporosity of TS-1 zeolite to construct a hierarchical structure, is another strategy to improve the diffusion efficiency.[14] To date, several different strategies, including the post-treatment method and hard/soft templates method, have been developed to effectively build the hierarchically porous system. Among them, the post-treatment method is a commonly used method that usually uses alkali treatment to remove the skeleton atoms to obtain a hierarchical structure.[15–17] It has been proven that TS-1 zeolite after alkali treatment exhibits excellent catalytic activity and high selectivity due to the hierarchical structure. However, the post-treatment process may lead to the loss of both skeleton silicon atoms and skeleton titanium species, which would change the original skeleton composition of TS-

[a] *National Laboratory for Clean Energy, Dalian Institute of Chemical Physics, Chinese Academy of Sciences, Dalian 116023, People's Republic of China. E-mail: zhangxm@dicp.ac.cn, leixu@dicp.ac.cn*
[b] *University of Chinese Academy of Sciences, Beijing 100049, People's Republic of China*

† Electronic supplementary information (ESI) available. See DOI: https://doi.org/10.1039/d4ce00706a

1 zeolite and even lead to a framework collapse.[18,19] For the hard-template method, carbon black, mesoporous carbon, sucrose, and other materials are usually used as hard templates.[20,21] Li *et al.* synthesized mesoporous TS-1 zeolite using carbon black as a hard-template agent and the zeolite showed high activity in the reaction of phenol hydroxylation and ammoxidation of methyl ethyl ketone.[22] Li *et al.* synthesized TS-1 with a well-connected network of mesopores and macropores using sucrose as a hard template, exhibiting high activity in the oxidation of bulky molecular benzothiophene.[23] However, some of the hard templates, especially the carbon materials, are usually prone to phase separation during the synthesis process, and thus leading to the inhomogeneity of the hierarchical structure and the catalytic active substances.[22] On the other hand, post-synthetic treatment usually involving high-temperature combustion for removing the hard templates made this traditional approach very complicated. For the soft-template method, polymers and organosilanes are commonly used as soft templates.[24] Yu *et al.* used Triton X-100 to synthesize hierarchical TS-1 with homogeneous mesopores in the crystal.[25] Shi *et al.* used CTAB as a mesoporous agent to prepare hierarchical TS-1. Compared with microporous TS-1, the mesoporous structure and weak hydrophobicity of this material make it exhibit higher catalytic activity and better recyclability in thiophene oxidation.[26] Unfortunately, the soft templates are usually not commercially available and costly. Therefore, tremendous efforts are usually made to design and synthesize such secondary templates before the construction of hierarchical zeolites, and the additional steps to remove templates will unavoidably bring about unwanted air pollution problems.[27]

Based on the above discussion, the hierarchical TS-1 zeolites are mostly synthesized using the hydrothermal synthesis method combined with additional templates or post-treatment steps. It is still difficult to synthesize hierarchical TS-1 zeolites in one pot without other additional templates in the hydrothermal synthesis system. To further simplify the synthesis procedure of hierarchical TS-1 zeolites, a constructive and facile steam-assisted crystallization (SAC) strategy has been developed.[28–32] Up to now, silicalite-1 and ZSM-5 with hierarchical structures have been synthesized based on the one-pot SAC strategy. Schwieger *et al.* fabricated a uniform macro/microporous silicalite-1 crystal by utilizing micro-sized mesoporous silica spheres as a silica source and sacrificial template for macropore formation.[33] Li *et al.* synthesized silicate-1 with different structures (nanoparticle size, smooth surface and coffin-like structure) by SAC by adjusting silicate sources.[34] Obviously, the absence of acidic sites in silicalite-1 would definitely limit their application in the catalysis field. Based on this, our group introduced Al species and ZSM-5 with hierarchical structures that were successfully synthesized.[31,35] Ryoo *et al.* used a dual-templating diquaternary ammonium surfactant for SAC synthesis of ZSM-5 nanosponges.[36] It can be seen that the SAC strategy presents obvious advantages compared with those for hierarchical zeolites mentioned above. Generally, the starting precursors could not only provide Si/Al sources for zeolite growth but also act as scaffold-like hard or soft templates. Therefore, the introduction of mesopores/macropores template and subsequent secondary processing steps were avoided. In addition, it has advantages such as less waste, lower structural directing agent (SDA) consumption, and smaller reactor volume.[33,34] Considering the same MFI structure of TS-1 zeolites with silicalite-1 and ZSM-5 zeolites and to further widen the application of zeolites, TS-1 zeolites with hierarchical structure are highly desired. Weissenberger *et al.* synthesized hierarchically structured TS-1 crystals with intracrystalline macropores by the SAC method and proposed an "inverse crystallisation" process.[37] Smeets *et al.* found that, after the SAC process, the poorly dispersed Ti species in the amorphous precursor particles are incorporated in the zeolitic framework in a highly dispersed tetrahedral Ti mode.[38] Soekiman *et al.* synthesized mesoporous titanium silicalite-1 (TS-1) with a higher content of active titanium in the framework (more than 5%).[39]

Herein, we report a SAC one-pot strategy for the construction of hierarchical TS-1 zeolites. In a typical synthesis, the $SiO_2$–$TiO_2$ precursor was prepared first and then transformed directly into hierarchical TS-1 zeolite through the SAC treatment. The Ti content of the prepared hierarchical TS-1 was tuned in a wide range. Moreover, the macroporous pore size of the hierarchical TS-1 zeolite was also tuned by changing the particle size of the $SiO_2$–$TiO_2$ precursor. The formation mechanism of hierarchical TS-1 zeolite was studied. The catalytic performance was tested in the epoxidation reaction of 1-hexene and the hydroxylation reaction of phenol. The present study is expected to provide a facile method to fabricate hierarchical TS-1 zeolite with a high content of framework Ti species.

## Experimental section

### Chemical and reagents

Cetyltrimethylammonium bromide (CTAB, 99%, Sinopharm Chemical Reagent Co., Ltd.), tetrapropylammonium hydroxide (TPAOH, 25 wt%, Gaoming Chemical Co.), ethanol (99%, Tianjin Fuyu Fine Chemical Co., Ltd.), ammonium hydroxide ($NH_3{\cdot}H_2O$, 25%, Damao Chemical Reagent Factory), tetraethyl orthosilicate (TEOS, 98%, Tianjin Kermel Chemical Reagent Co., Ltd.), tetrabutyl titanate (TBOT, 98%, Damao Chemical Reagent Factory), isopropyl alcohol (IPA, 99%, Guangdong Guanghua Sci-Tech Co., Ltd.), 1-hexene (99%, Shanghai Aladdin Reagents Co., Ltd.), methanol (99%, Shandong Yuwang Hetianxia New Materials Co., Ltd.), phenol (99%, Guangdong Guanghua Sci-Tech Co., Ltd.), 1,3,5-trimethyl benzene (98%, Shanghai Aladdin Reagents Co., Ltd.), 1-propanol (99%, Xilong Scientific Co., Ltd.), hydrogen peroxide ($H_2O_2$, 99%, Damao Chemical Reagent Factory). All reagents were used without further purification.

 

### Synthesis of $SiO_2$–$TiO_2$ precursor

**The $SiO_2$–$TiO_2$ precursor was prepared as follows.** CTAB was dissolved into a mixture of deionized water and anhydrous ethanol. A certain amount of ammonia was added to tune the solution pH in the range of 9–11. After stirring at 323 K for 0.5 h, certain content of TEOS and TBOT were slowly added to the above mixture and then continued to stir at 323 K for another 1.5 h. The final products were centrifuged, washed, dried at 353 K, and calcined at 823 K for 6 h to remove CTAB. By changing the ratio of deionized water and anhydrous ethanol, the $SiO_2$–$TiO_2$ precursor with different particle sizes was obtained and denoted as $SiO_2$–$TiO_2$($x$), where $x$ is the particle size of the precursor.

### Synthesis of hierarchical TS-1

**The preparation process of hierarchical TS-1 *via* SAC strategy was as follows.** A certain amount of $SiO_2$–$TiO_2$ precursor was impregnated with TPAOH solution. The mixture was left at room temperature overnight and the excess water was removed in an oven at 313 K to adjust the composition of dry gel to 1.0 $SiO_2$ : 0.2 TPAOH : 1.0 $H_2O$. The solid dry gel was then ground into powder, transferred to a Teflon-made tray, and sealed into a Teflon-lined stainless-steel autoclave with some deionized water added into the bottom of the autoclave. After crystallization at 443 K for 36 h, the solid products were washed with ethanol and deionized water 3 times, dried overnight in an oven at 353 K, and then calcined at 823 K for 6 h. The obtained products were denoted as HTS-1($y$), where $y$ is the silicon-to-titanium ratio of the $SiO_2$–$TiO_2$ precursor.

**Tuning the pore size of the macropores.** $SiO_2$–$TiO_2$(150) and $SiO_2$–$TiO_2$(400) with a Si/Ti ratio of 50 were used as the precursor for tuning the pore size of the macropores, and their corresponding zeolite products were denoted as HTS-1(50)-A and HTS-1(50)-B, respectively.

### Synthesis of conventional microporous TS-1

Conventional microporous TS-1 was prepared by conventional hydrothermal method with gel composition of 1.0 $SiO_2$ : 0.02 $TiO_2$ : 0.15 TPAOH : 60 $H_2O$. The specific preparation process was as follows: firstly, TPAOH and TEOS were added to deionized water successively, followed by stirring for 0.5 h at room temperature. TBOT was then slowly added to the above solution and continued to be stirred for 1 h. After that, the solution was stirred at 353 K for 3 h, and after adding deionized water to the target amount, it was transferred to the Teflon-lined stainless-steel autoclave and crystallized at 453 K for 36 h. The obtained solid products were centrifuged, washed, and dried in an oven at 353 K, then calcined in a muffle furnace at 823 K for 6 h to remove TPAOH. The obtained product was denoted as CTS-1(50).

### Characterization

Powder X-ray diffraction (XRD) patterns of samples were recorded to determine the crystal phase on the PANalytical X'pert Pro-1 diffractometer with Cu-Kα radiation. The morphologies and particle size of samples were observed by scanning electron microscopy (SEM, JSM-7800F) and transmission electron microscopy (TEM, JEM-2100). The textual properties of the samples were examined by Micromeritics ASAP 2460 Surface Area and Porosity Analyzer at 77 K. Prior to the measurement, the samples were outgassed at 623 K for 10 h. Brauner–Emmett–Teller (BET) equation was adopted for total surface areas calculation. *T*-Plot method was applied to the calculation of micropore surface areas and micropore volumes. The inductively coupled plasma optical emission spectroscopy (ICP-OES) was determined by Optima 7300DV spectrometer for Ti content analysis. The ultraviolet-visible diffuse reflectance spectroscopy (UV-vis) of samples were collected by SHIMADZU UV2600 with a spectral scanning range between 200–800 nm to determine the Ti species. Fourier transform infrared spectra (FT-IR) of samples were obtained by Thermo Fisher Scientific Nicolet iS50 with spectral scanning range between 400–4000 $cm^{-1}$.

### Catalytic performance testing

The epoxidation reaction of 1-hexene (1-Hex) was carried out in a single-necked round bottom flask equipped with a reflux condenser and a magnetic stirring device. The specific steps of the reaction evaluation were as follows: 200 mg of catalyst, 40 mL of methanol, 40 mmol of $H_2O_2$ (30 wt%), and 40 mmol of 1-hexene were added into the round bottom flask. Then the above mixture was vigorously stirred at 333 K for 2 h. After the reaction was completed and cooled to room temperature, the internal standard 1,3,5-trimethyl benzene was added and stirred evenly.

The product was analyzed by an Agilent 7890A gas chromatography equipped with a SE-54 capillary column (30 m × 0.25 mm × 0.25 μm) and a hydrogen flame ionization detector (FID). The conversion of 1-hexene and the selectivity of 1,2-epoxyhexane (1,2-Epo) were quantitatively calculated by the internal standard method. At the same time, the remaining $H_2O_2$ was measured by the iodometric method to calculate the conversion of $H_2O_2$.

The hydroxylation reaction of phenol (Phe) was carried out in a single-necked round bottom flask equipped with a reflux condenser and a magnetic stirring device. In a typical procedure, 300 mg of catalyst, 4 mL of deionized water, 36 mmol of phenol and 18 mmol of $H_2O_2$ (30 wt%) were added to the round bottom flask. Then the above mixture was vigorously stirred at 353 K for 1 h. After the reaction was completed and cooled to room temperature, the internal standard *n*-propanol was added and stirred evenly.

The products were analyzed using an Agilent 7890A gas chromatography equipped with a SE-54 capillary column (30 m × 0.25 mm × 0.25 μm) and a hydrogen flame ionization

detector (FID). The conversion of phenol, and the selectivity of hydroquinone (HQ), catechol (CAT) and benzoquinone (BQ) were quantitatively calculated by internal standard method. At the same time, the iodometric method was used to measure the conversion of $H_2O_2$.

The calculation formula is as follows:

$$X(\text{1-Hex}) = 1 - n(\text{1-Hex})/n_0(\text{1-Hex})$$

$$S(\text{1,2-Epo}) = n(\text{1,2-Epo})/(n(\text{1,2-Epo}) + n(\text{Other}))$$

$$X(\text{Phe}) = 1 - n(\text{Phe})/(n(\text{Phe}) + n(\text{CAT}) + n(\text{HQ}) + n(\text{BQ}))$$

$$S(\text{HQ}) = n(\text{HQ})/(n(\text{CAT}) + n(\text{HQ}) + n(\text{BQ}))$$

$$S(\text{CAT}) = n(\text{CAT})/(n(\text{CAT}) + n(\text{HQ}) + n(\text{BQ}))$$

$$S(\text{BQ}) = n(\text{BQ})/(n(\text{CAT}) + n(\text{HQ}) + n(\text{BQ}))$$

$$X(\text{H}_2\text{O}_2) = (n_0(\text{H}_2\text{O}_2) - n(\text{H}_2\text{O}_2))/n_0(\text{H}_2\text{O}_2)$$

## Results and discussion

### Preparation and characterization of hierarchical TS-1 zeolites

In general, the synthesis process of hierarchical TS-1 zeolites included two key steps. First of all, $SiO_2$–$TiO_2$(200) precursors with a uniform size of about 200 nm (Fig. 4A) were prepared as the starting materials for the synthesis of hierarchical TS-1 zeolites. Then, the $SiO_2$–$TiO_2$(200) precursor was treated *via* SAC strategy after being impregnated with a certain amount of TPAOH solution, and hierarchical TS-1 zeolites could be obtained finally. The Si/Ti ratios of the obtained TS-1 zeolites could be tuned in a range of 30 to 90 by simply varying the initial content of Ti in the $SiO_2$–$TiO_2$(200) precursor. To compare the synthesis process and catalytic performance with hierarchical TS-1 zeolites, conventional TS-1 samples with a Si/Ti ratio of 50, denoted as CTS-1-(50), were also synthesized using the hydrothermal synthesis method.

XRD patterns of the obtained samples are shown in Fig. 1A. As clearly shown, no diffraction peaks were observed in the XRD pattern, indicating that $SiO_2$–$TiO_2$(200) precursor has an amorphous phase (Fig. 4F). All the zeolite samples show typical diffraction peaks at $2\theta$ = 7.9°, 8.8°, 23.1°, 23.9° and 24.4°, indicating the formation of pure MFI phase (Fig. 1A). Besides, no splitting peaks were detected at $2\theta$ = 24.4°and 29.3°, which indicates the transformation from monoclinic phase (Silicate-1) to orthogonal phase caused by the inserting of Ti into MFI framework,[40–42] suggesting that TS-1 zeolite was obtained.

To further investigate the form of Ti species in HTS-1($x$) samples, UV-vis and FT-IR characterization were performed. UV-vis spectroscopy is one of the first spectral techniques used for the detection of coordination states of Ti species in TS-1 zeolite. As shown in Fig. 1B, only a strong absorption peak located at 210–220 nm was discovered for all the zeolites samples, which originated from the transition between 2p electrons of oxygen atom in the TS-1 framework and the 3d empty orbit of the tetra-coordinated framework Ti species.[43] This result indicates that only tetra-coordinated framework Ti species exist in these TS-1 zeolites. For HTS-1(30), the UV-vis spectra exhibited a weak absorption peak at 320 nm besides the absorption peak at 210–220 nm. It represents that only a portion of titanium atoms in HTS-1(30) are inserted into the skeleton to form four coordinated titanium species while the remaining titanium atoms form extra-framework anatase $TiO_2$ due to the much higher content of Ti species.

FT-IR spectra are shown in Fig. 1C. Compared with the $SiO_2$–$TiO_2$(200) precursor, new bands at 550, 960 and 1225 $cm^{-1}$ appeared in the FT-IR spectra of TS-1 samples. The bands at 550 and 1225 $cm^{-1}$ are ascribed to the double five-membered rings and asymmetric stretching vibration mode of the MFI molecular sieve, demonstrating the formation of

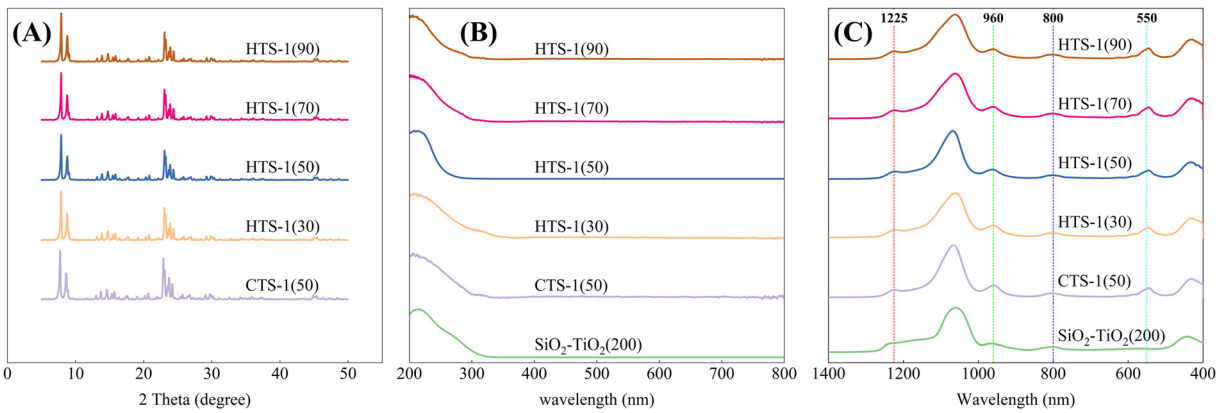


Fig. 1 (A) XRD patterns, (B) UV-vis spectra, (C) FT-IR spectra of the $SiO_2$–$TiO_2$ precursor, HTS-1($x$) samples and CTS-1(50).

 

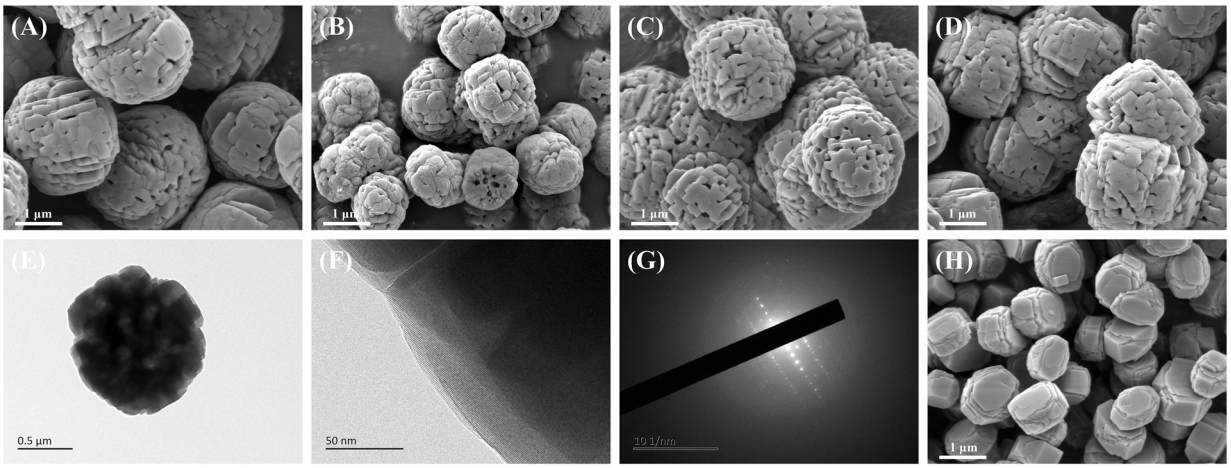


Fig. 2 (A–D) SEM images of HTS-1(30), HTS-1(50), HTS-1(70) and HTS-1(90), (E–G) TEM, HR-TEM and SAED images of HTS-1(50), (H) SEM images of CTS-1(50).

the MFI structure.[43–45] The band presented at 960 $cm^{-1}$ belongs to the perturbation of Si–O bands by adjacent Ti atoms, indicating the formation of Si–O–Ti bonds, which means that Ti atoms were successfully inserted into the framework to form TS-1 zeolite.[46,47] These results are consistent with the UV-vis spectroscopy analysis.

SEM and TEM results of HTS-1($x$) samples and CTS-1(50) are shown in Fig. 2. The $SiO_2$–$TiO_2$(200) precursor (Fig. 4A) consisted of relatively uniform spheroidal crystals and smooth surface with dimensions of about 200 nm.

HTS-1(50) exhibits a relatively uniform spheroidal morphology with a particle size of around 1.2 μm (Fig. 2B). Obviously, macropores with diameters of about 110 nm could be identified on the particle surface (Fig. S1†). The TEM result shown in Fig. 2E clearly displayed the existence of macropores with a pore size of about 150 nm, which is slightly larger than the 110 nm observed in the SEM image.

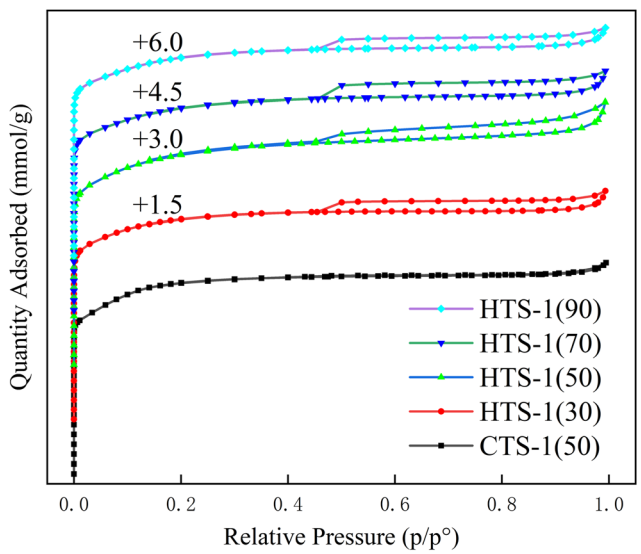


Fig. 3 $N_2$ adsorption/desorption isotherms of HTS-1($x$) samples and CTS-1(50).

Well-defined lattice fringes of the same orientation observed in HR-TEM images (Fig. 2F) and discrete diffraction spots detected in the SAED images (Fig. 2G) gave further evidence of high crystalline degree. According to the SEM and TEM characterization, hierarchical TS-1 with even macropores was obtained. As shown in Fig. 2A, C and D, the series of hierarchical TS-1 zeolites, including HTS-1(30), HTS-1(70) and HTS-1(90), show a similar morphology rich in macropores. In contrast, the CTS-1(50) sample possesses a uniform regular hexagonal prism morphology with a particle size of around 1.1 μm and a smooth surface (Fig. 2H). No mesopores or macropores were detected in CTS-1(50).

$N_2$ physisorption characterization was performed to analyze the texture properties of HTS-1($x$) samples and CTS-1(50). Based on IUPAC classification, HTS-1($x$) samples possess type IV sorption isotherms, which indicates the feature of mesoporous materials (Fig. 3).

A rapid increase of nitrogen adsorption capacity at $P/P_0 < 0.01$ arising from the 10-member ring channels indicates the presence of intrinsic micropores of MFI framework. The obvious H4 hysteresis loop presented at $P/P_0 > 0.45$ reveals the presence of mesopores or micropores. The appearance of the hysteresis loop at $P/P_0$ = 0.4–0.8 is related to intracrystalline mesopores, suggesting that intracrystalline mesopores were probably formed in HTS-1($x$) samples. CTS-1(50) exhibits the characteristics of type I sorption isotherms, and it also shows the rapid uptake of $N_2$ adsorption in the low relative pressure range ($P/P_0$ = 0–0.1), indicating the existence of abundant micropores. Unlike the HTS-1($x$) samples, the $N_2$ sorption isotherms of CTS-1(50) have no hysteresis loop in the high relative pressure range ($P/P_0 > 0.45$), indicating that almost no mesopores or macropores existed for CTS-1(50). This result is consistent with the SEM and TEM characterization results.

The textural properties of CTS-1(50) and HTS-1($x$) samples are summarized in Table 1. In comparison with CTS-1(50), HTS-1($x$) samples with hierarchical structure has larger specific surface area and pore volume owing to the

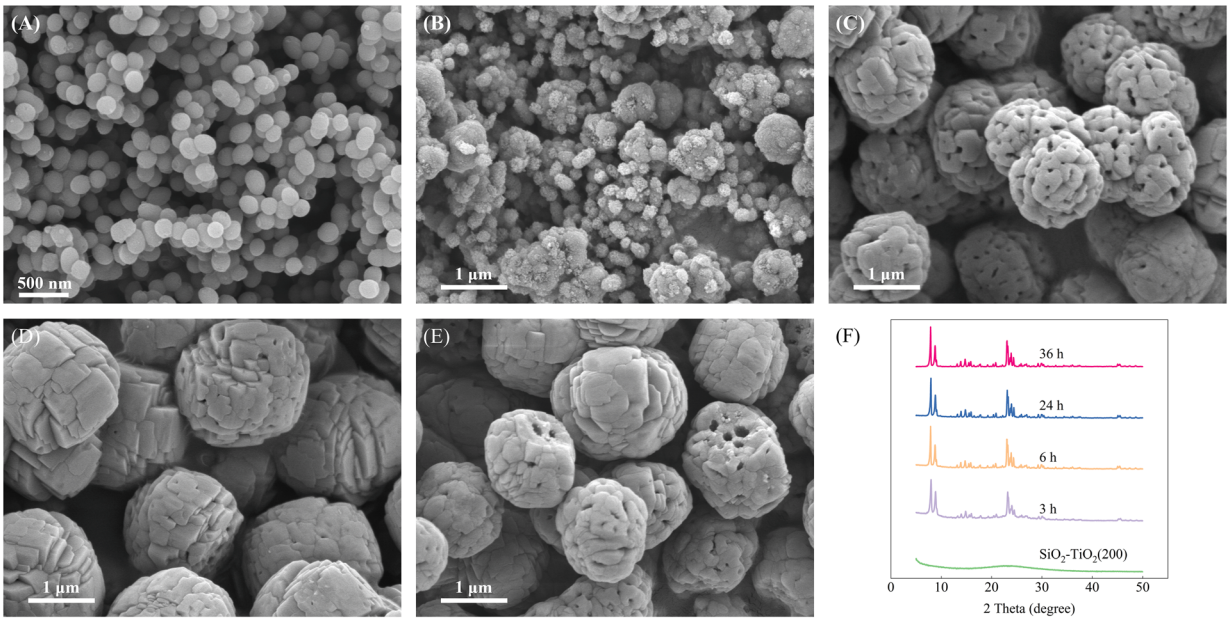


Fig. 4 Study on crystallization process of HTS-1: SEM images of HTS-1(50) samples crystallized at 0 h (A), 3 h (B), 6 h (C), 24 h (D) and 36 h (E); XRD patterns of the samples obtained at different crystallization times (F).

Table 1 Textural properties of samples

| Sample | Ti (wt%) | Surface areas ($m^2$ $g^{-1}$) | | | Pore volumes ($cm^3$ $g^{-1}$) | | |
|---|---|---|---|---|---|---|---|
| | | Total | Micropore | External | Total | Micropore | Mesopore |
| $SiO_2$–$TiO_2$(200) | 1.36 | 979 | 871 | 108 | 0.78 | 0.62 | 0.16 |
| CTS-1(50) | 1.38 | 459 | 454 | 5 | 0.21 | 0.19 | 0.02 |
| HTS-1(30) | 1.39 | 484 | 479 | 5 | 0.23 | 0.20 | 0.03 |
| HTS-1(50) | 1.34 | 499 | 478 | 21 | 0.26 | 0.21 | 0.05 |
| HTS-1(70) | 1.00 | 486 | 477 | 9 | 0.24 | 0.20 | 0.04 |
| HTS-1(90) | 0.70 | 474 | 466 | 8 | 0.23 | 0.20 | 0.03 |
| HTS-1(50)-A | 1.31 | 477 | 449 | 28 | 0.24 | 0.19 | 0.05 |
| HTS-1(50)-B | 1.30 | 471 | 455 | 16 | 0.22 | 0.19 | 0.03 |

contribution from both mesopores and macropores (Table 1), especially the HTS-1(50) zeolite (499 $m^2$ $g^{-1}$ *vs.* 459 $m^2$ $g^{-1}$ and 0.26 $m^3$ $g^{-1}$ *vs.* 0.21 $m^3$ $g^{-1}$).

### Formation mechanism analysis of the hierarchical HTS-1

To understand the formation mechanism of hierarchical structure during the transformation process of the $SiO_2$–$TiO_2$ precursor into HTS-1($x$) samples, HTS-1(50) as a representative sample obtained at different crystallization times was analyzed by means of SEM and XRD. As shown in Fig. 4A, the $SiO_2$–$TiO_2$(200) precursor started to dissolve at the very beginning of the crystallization process (3 h), and its surface became rough.

The particle size decreased obviously suggesting the dissolution of the $SiO_2$–$TiO_2$(200) precursor. Then, little crystals grew around the partially dissolved $SiO_2$–$TiO_2$(200) precursor. No significant crystals were formed and typical diffraction peaks of MFI topological structure with low intensity appeared at this stage (Fig. 4F), which was consistent with the corresponding SEM image. When the crystallization proceeded to 6 h, the $SiO_2$–$TiO_2$(200) precursor completely disappeared (Fig. 4C), and crystallized products rich in macropores emerged. The intensity of the diffraction peak in the XRD pattern was greatly enhanced compared to that of 3 h. As the crystallization time prolonged from 6 h to 36 h (Fig. 4C–E), the crystal size did not change significantly, while the macropores embedded in the surface decreased slightly, which may be related to Ostwald ripening.[48]

On the basis of the above analysis results, the formation process of HTS-1 can be summarized as follows. In the early stage of crystallization, the $SiO_2$–$TiO_2$(200) precursor dissolved outside-in under the etching effect of TPAOH. At the same time, the dissolved silica and titanium species crystallized *in situ* with the aid of the structure-directing agent TPAOH. The crystals gradually grew and wrapped the incompletely dissolved precursor, resulting in the appearance of precursors "embedded" in the crystals. With the prolongation of the crystallization time, the $SiO_2$–$TiO_2$(200) precursor dissolved completely, and smallish holes were left in their original positions. Finally, hierarchical HTS-1 with

 

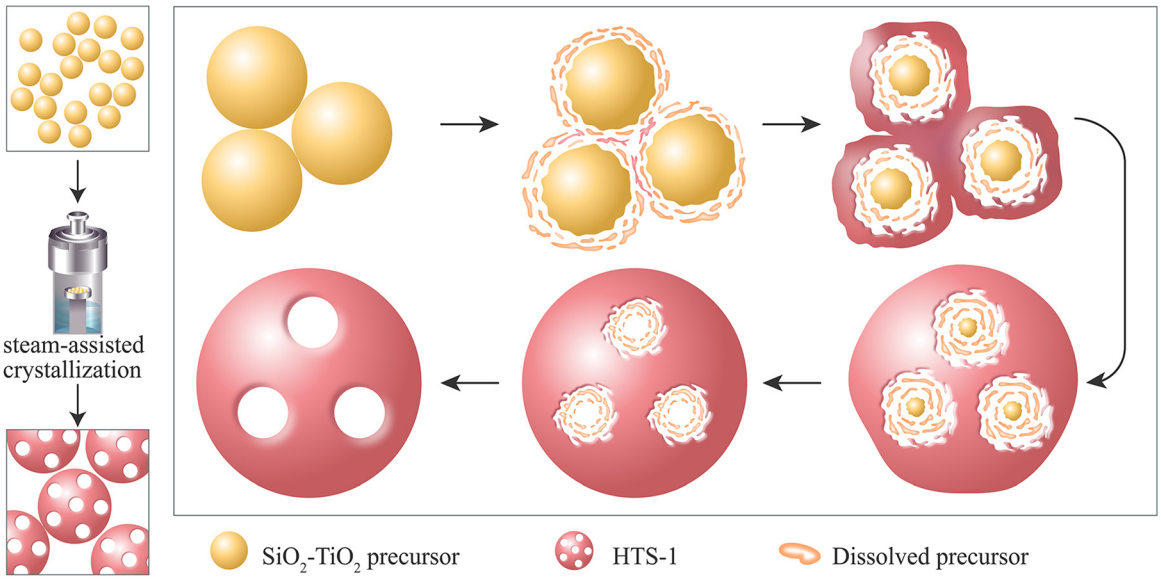


**Scheme 1** The formation procedure of HTS-1.

macropores was formed (Scheme 1). The mechanism we proposed here is different from the liquid-phase mechanism in Xiong's work.[49] Although amorphous $SiO_2$–$TiO_2$ was crystallized into TS-1 zeolite in that work, the SAC strategy was not adopted, and the hierarchical morphology was not obtained.

### Regulation of the pore size of macropores

According to the understanding of the formation mechanism of the macropores in the HTS-1 zeolite, it can be speculated that the particle size of the precursor could influence the pore size of macropores. To adjust the pore size and further verify the reliability of the proposed mechanism, $SiO_2$–$TiO_2$(150) and $SiO_2$–$TiO_2$(400) precursors were synthesized (Fig. 5A and D, respectively). The corresponding products denoted as HTS-1(50)-A and HTS-1(50)-B were synthesized and characterized. The results and analysis are shown below.

Fig. S2† shows the XRD, UV-vis and FT-IR characterization results of HTS-1(50)-A and HTS-1-(50)-B, which suggest that TS-1 zeolite was obtained. As shown in Fig. 5, abundant macropores exist in HTS-1(50)-A and HTS-1-(50)-B. The macropores on the surface of HTS-1(50)-A were fewer and the pore size are as small as approximately 70 nm (Fig. 5B, C and S3A†).

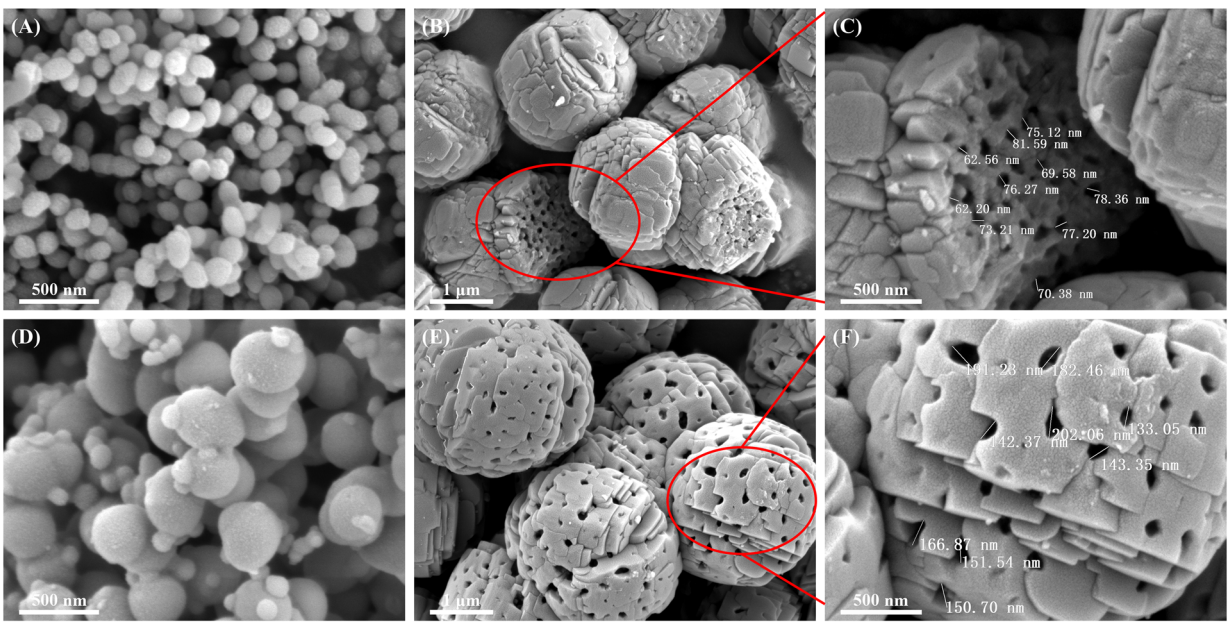


**Fig. 5** SEM images of $SiO_2$–$TiO_2$(150) (A), HTS-1-(50)-A (B and C), $SiO_2$–$TiO_2$(400) (D) and HTS-1(50)-B (E and F).

While for HTS-1-(50)-B, the surface has an abundance of macropores with the size of 130–200 nm (Fig. 5C, D and S3B†). The macropore size was much larger than that of HTS-1-(50) and HTS-1-(50)-A. The main reason for the obvious macropores size change was the initial particle size of the precursors. Based on these results it can be concluded that the macropores size of HTS-1 zeolite could be tuned easily through the change of the particle size of the precursor, which is consistent with the crystallization mechanism proposed above. All in all, the strategy proposed in this manuscript provides a facile method for adjusting the pore size of the hierarchical TS-1 zeolites in one pot.

### Catalytic performance

The combination of a hierarchical structure and anatase-free TS-1 zeolite contributes to promising catalytic performance, especially when macromolecule substrates are involved in catalytic reactions. In the present work, the epoxidation of 1-hexene and hydroxylation of phenol were carried out respectively to evaluate the performance of the synthesized TS-1 zeolites. As a comparison, conventional TS-1 zeolite with similar particle size and similar Si/Ti ratio was also tested under the same conditions. It can be seen from Table 2 that in the epoxidation of 1-hexene, the reaction activity of HTS-1(50), HTS-1(50)-A and HTS-1-(50)-B was higher than that of CTS-1(50) (21.0%, 20.1%, and 19.3% *vs.* 18.3%), but the performance difference is not significant. This result might come from the fact that compared with the microporous channel structure of CTS-1(50), the introduction of macropores in HTS-1(50), HTS-1(50)-A and HTS-1-(50)-B does not significantly improve the mass transfer efficiency of small molecules such as 1-hexene.

When they were applied to the phenol hydroxylation reaction, the performance advantage of HTS-1(50), HTS-1(50)-A and HTS-1-(50)-B over CTS-1(50) was enhanced. Under the same conditions, HTS-1(50) exhibited the highest conversion of phenol. Besides, HTS-1(50), HTS-1(50)-A and HTS-1-(50)-B show higher selectivity in HQ compared with CTS-1(50). However, the performance over CTS-1(50) was much lower than that of hierarchical TS-1 zeolites through the comparative Ti content. Therefore, the improved catalytic performance of the hierarchical TS-1 zeolites probably originates from the improved diffusion efficiency. The hierarchical structure greatly alleviates the diffusion limitation of macromolecular and increases the accessibility of active sites, thereby achieving the purpose of improving the reaction performance.

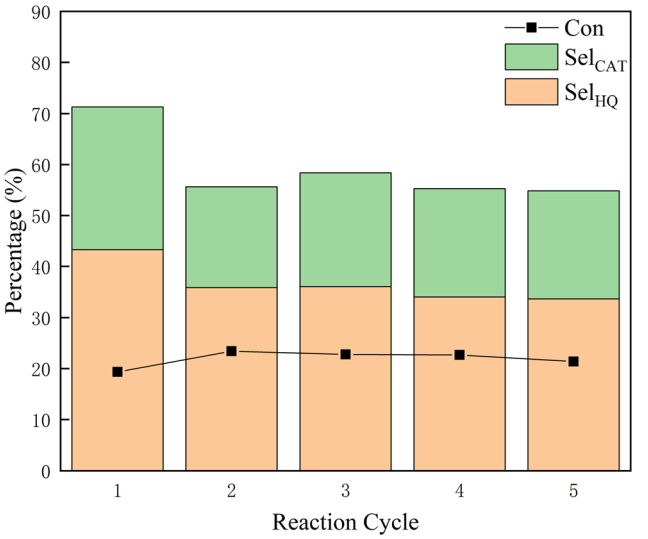


Fig. 6 Recycling experiments of the phenol hydroxylation reaction by HTS-1(50).

The stability of hierarchical TS-1 zeolite was tested in a phenol hydroxylation reaction. After each run, the spent HTS-1(50) was separated by centrifugation and calcined at 823 K for 6 h in air. As shown in Fig. 6, the conversion of phenol and the selectivity of CAT and HQ remained essentially stable during the following five runs, suggesting the excellent stability of the synthesized TS-1 zeolite which is one of the key features for practical applications in the industry.

## Conclusions

In summary, a facile one-pot stream-assisted crystallization strategy has been developed for the synthesis of anatase-free hierarchical TS-1 zeolite with abundant macropores and

Table 2 Catalytic performance of CTS-1(50) and HTS-1(*x*) samples in 1-hexene epoxidation and phenol hydroxylation

| | 1-Hexene epoxidation[a] | | | Phenol hydroxylation[b] | | | | |
|---|---|---|---|---|---|---|---|---|
| Sample | Conv. (%) | Sel. (%) | $X_{H_2O_2}$ (%) | Conv. (%) | $S_{HQ}$ (%) | $S_{CAT}$ (%) | $S_{BQ}$ (%) | $X_{H_2O_2}$ (%) |
| CTS-1(50) | 18.3 | 98.2 | 22.2 | 14.3 | 27.6 | 19.2 | 53.2 | 18.9 |
| HTS-1(30) | 21.4 | 98.5 | 23.6 | 24.0 | 40.1 | 21.2 | 38.7 | 57.7 |
| HTS-1(50) | 21.0 | 98.4 | 22.6 | 33.6 | 45.4 | 31.2 | 23.4 | 72.9 |
| HTS-1(70) | 15.2 | 97.5 | 18.0 | 19.1 | 40.8 | 21.3 | 37.9 | 44.2 |
| HTS-1(90) | 12.0 | 96.9 | 12.9 | 18.4 | 38.6 | 22.5 | 38.9 | 26.9 |
| HTS-1(50)-A | 20.1 | 98.3 | 20.2 | 22.7 | 45.4 | 28.0 | 26.6 | 45.0 |
| HTS-1(50)-B | 19.3 | 98.3 | 22.6 | 19.3 | 43.3 | 28.0 | 28.7 | 45.1 |

[a] Cat., 200 mg; 1-hexene, 40 mmol; $H_2O_2$ (30 wt%), 40 mmol; methanol, 40 mL; temp., 333 K; time, 2 h. [b] Cat., 300 mg; $n$(phenol) : $n(H_2O_2)$ = 2; phenol, 36 mmol; $H_2O_2$ (30 wt%), 18 mmol; $H_2O$, 4 mL; temp., 353 K; time, 1 h.

 

tunable macropores size. The role of amorphous $SiO_2$–$TiO_2$ precursor as the titanium–silicon species and macropore template in the crystallization process of TS-1 zeolite was essential to construct hierarchical pores. The Ti content of the hierarchical TS-1 was tuned in a wide range by varying the Ti content of the precursor. It has been demonstrated that bigger $SiO_2$–$TiO_2$ precursor spheres could generate bigger macropores in the hierarchical TS-1 crystals. The hierarchical TS-1 zeolite gave better reaction activity in the epoxidation of 1-hexene and phenol hydroxylation compared to the conventional TS-1 due to the improved diffusion efficiency originating from the hierarchical texture. Moreover, the TS-1 zeolites exhibited high stability in the phenol hydroxylation reaction. This work may provide a promising strategy for the synthesis of hierarchical TS-1 zeolite with adjustable pore size.

## Data availability

The data supporting this article have been included as part of the ESI.†

## Conflicts of interest

There are no conflicts to declare.

## Acknowledgements

This work was financially supported by National Key R&D Program of China (2021YFA1501900).

## Notes and references

1 M. Taramasso, G. Perego and B. Notari, *US Pat.*, 4410501, 1983.
2 M. Liu, J. Li, X. Chen, J. Song, W. Wei, Y. Wen and X. Wang, *Microporous Mesoporous Mater.*, 2021, **326**, 111388.
3 G. Xiong, Y. Cao, Z. Guo, Q. Jia, F. Tian and L. Liu, *Phys. Chem. Chem. Phys.*, 2016, **18**, 190–196.
4 J. Wang, X. Shen, Y. Zhang, J. Lu, M. Liu, L. Ling, J. Liao, L. Chang and K. Xie, *Mol. Catal.*, 2022, **532**, 112744.
5 S.-T. Tsai, P.-Y. Chao, T.-C. Tsai, I. Wang, X. Liu and X.-W. Guo, *Catal. Today*, 2009, **148**, 174–178.
6 C. Niu, X. Yang, Q. Zhang, Y. Zhang, X. Qin, Y. Tang, H. Wei, X. Gao, Y. Liu, X. Wang, Y. Wen and F.-S. Xiao, *Microporous Mesoporous Mater.*, 2023, **351**, 112467.
7 R. J. Lewis, K. Ueura, X. Liu, Y. Fukuta, T. E. Davies, D. J. Morgan, L. Chen, J. Qi, J. Singleton, J. K. Edwards, S. J. Freakley, C. J. Kiely, Y. Yamamoto and G. J. Hutchings, *Science*, 2022, **376**, 615–620.
8 S. Du, H.-M. Chen, H.-X. Shen, J. Chen, C.-P. Li and M. Du, *ACS Appl. Nano Mater.*, 2020, **3**, 9393–9400.
9 R. Bai, Y. Song, G. Tian, F. Wang, A. Corma and J. Yu, *Green Energy Environ.*, 2023, **8**, 163–172.
10 Q. Lv, G. Li and H. Sun, *Fuel*, 2014, **130**, 70–75.
11 A. Silvestre-Albero, A. Grau-Atienza, E. Serrano, J. García-Martínez and J. Silvestre-Albero, *Catal. Commun.*, 2014, **44**, 35–39.
12 M. Liu, Z. Chang, H. Wei, B. Li, X. Wang and Y. Wen, *Appl. Catal., A*, 2016, **525**, 59–67.
13 Y. Zuo, M. Liu, T. Zhang, C. Meng, X. Guo and C. Song, *ChemCatChem*, 2015, **7**, 2660–2668.
14 S. L. Suib, J. Prech, E. Szaniawska and J. Cejka, *Chem. Rev.*, 2023, **123**, 877–917.
15 Y. Zuo, L. Yang, X. Jiang, M. Ma, Y. Wang, M. Liu, C. Song and X. Guo, *ChemCatChem*, 2020, **12**, 6196–6204.
16 L. Chen, X. Zhang, Q. Han, L. Xu, S. Zhang, Y. Yuan and L. Xu, *Appl. Catal., A*, 2020, **598**, 117588.
17 C. Miao, Q. Zhu, Y. Yi, J. Su, N. He, J. Liu and H. Guo, *Ind. Eng. Chem. Res.*, 2019, **58**, 11739–11749.
18 M. Zhang, S. Ren, Q. Guo and B. Shen, *Microporous Mesoporous Mater.*, 2021, **326**, 111395.
19 G. Lv, S. Deng, Y. Zhai, Y. Zhu, H. Li, F. Wang and X. Zhang, *Appl. Catal., A*, 2018, **567**, 28–35.
20 C. J. H. Jacobsen, C. Madsen, J. Houzvicka, I. Schmidt and A. Carlsson, *J. Am. Chem. Soc.*, 2000, **122**, 7116–7117.
21 Y. Fang and H. Hu, *Catal. Commun.*, 2007, **8**, 817–820.
22 H. Xin, J. Zhao, S. Xu, J. Li, W. Zhang, X. Guo, E. J. M. Hensen, Q. Yang and C. Li, *J. Phys. Chem. C*, 2010, **114**, 6553–6559.
23 W. Wang, G. Li, L. Liu and Y. Chen, *Microporous Mesoporous Mater.*, 2013, **179**, 165–171.
24 Y. Cheneviere, F. Chieux, V. Caps and A. Tuel, *J. Catal.*, 2010, **269**, 161–168.
25 S. Du, F. Li, Q. Sun, N. Wang, M. Jia and J. Yu, *Chem. Commun.*, 2016, **52**, 3368–3371.
26 Y. Zhu, Z. Hua, X. Zhou, Y. Song, Y. Gong, J. Zhou, J. Zhao and J. Shi, *RSC Adv.*, 2013, **3**, 4193–4198.
27 Q. Du, Y. Guo, H. Duan, H. Li, Y. Chen and H. Liu, *Fuel*, 2017, **188**, 232–238.
28 P.-Y. Chao, W.-T. Chen, Y.-S. Lin, H.-Y. Hsu, H. Asakura, T. Tanaka and T.-C. Tsai, *Catal. Today*, 2020, **355**, 180–187.
29 Z. Kong, B. Yue, W. Deng, K. Zhu, M. Yan, Y. Peng and H. He, *Appl. Organomet. Chem.*, 2014, **28**, 239–243.
30 W. Song, Z. Liu, L. Liu, A. L. Skov, N. Song, G. Xiong, K. Zhu and X. Zhou, *RSC Adv.*, 2015, **5**, 31195–31204.
31 Y. Zhang, P. Lu, Y. Yuan, L. Xu, H. Guo, X. Zhang and L. Xu, *CrystEngComm*, 2017, **19**, 4713–4719.
32 L. Xu, Y. Yuan, J. Zhang, Y. Zhang, X. Zhang, L. Chen and L. Xu, *CrystEngComm*, 2020, **22**, 945–954.
33 A. G. Machoke, A. M. Beltrán, A. Inayat, B. Winter, T. Weissenberger, N. Kruse, R. Güttel, E. Spiecker and W. Schwieger, *Adv. Mater.*, 2015, **27**, 1066–1070.
34 J. Zhang, X. Li, J. Liu and C. Wang, *Catalysts*, 2019, **9**, 13.
35 Y. Zhang, X. Zhang, J. Zhang, P. Li, Q. Han, L. Xu and H. Guo, *CrystEngComm*, 2018, **20**, 6786–6794.
36 S. W. Han, J. Kim and R. Ryoo, *Microporous Mesoporous Mater.*, 2017, **240**, 123–129.
37 T. Weissenberger, R. Leonhardt, B. A. Zubiri, M. Pitínová-Štekrová, T. L. Sheppard, B. Reiprich, J. Bauer, R. Dotzel, M. Kahnt, A. Schropp, C. G. Schroer, J.-D. Grunwaldt, J. L.

Casci, J. Čejka, E. Spiecker and W. Schwieger, *Chem. – Eur. J.*, 2019, **25**, 14430–14440.
38 V. Smeets, E. M. Gaigneaux and D. P. Debecker, *Microporous Mesoporous Mater.*, 2020, **293**, 109801.
39 C. N. Soekiman, K. Miyake, Y. Hayashi, Y. Zhu, M. Ota, H. Al-Jabri, R. Inoue, Y. Hirota, Y. Uchida, S. Tanaka, C. Y. Kong and N. Nishiyama, *Mater. Today Chem.*, 2020, **16**, 100209.
40 F. Jin, X. Wang, T. Liu, L. Xiao, M. Yuan and Y. Fan, *Chin. J. Chem. Eng.*, 2017, **25**, 1303–1313.
41 Y. Jiao, A.-L. Adedigba, N. F. Dummer, J. Liu, Y. Zhou, Y. Guan, H. Shen, M. Perdjon and G. J. Hutchings, *Microporous Mesoporous Mater.*, 2020, **305**, 110397.
42 M. Du, G. Zhan, X. Yang, H. Wang, W. Lin, Y. Zhou, J. Zhu, L. Lin, J. Huang, D. Sun, L. Jia and Q. Li, *J. Catal.*, 2011, **283**, 192–201.
43 G. An, C. A. Wang, H. Gao, G. Wang, Y. Luo, Z. Liu, C. Xia, S. Liu, X. Peng, Z. Cheng and X. Shu, *J. Colloid Interface Sci.*, 2023, **633**, 291–302.
44 S. P. Naik, A. S. T. Chiang, R. W. Thompson and F. C. Huang, *Chem. Mater.*, 2003, **15**, 787–792.
45 Z. Chen, J. Wang, K. Shen, R. Wang, H. Liu, X. Huang, Z. Tang, Y. Yu and Y. Liu, *Appl. Catal., A*, 2020, **591**, 117403.
46 J. Klaas, K. Kulawik, G. Schulz-Ekloff and N. I. Jaeger, in *Studies in Surface Science and Catalysis*, ed. J. Weitkamp, H. G. Karge, H. Pfeifer and W. Hölderich, Elsevier, 1994, vol. 84, pp. 2261–2268.
47 J. Zhang, R. Bai, Y. Zhou, Z. Chen, P. Zhang, J. Li and J. Yu, *Chem. Sci.*, 2022, **13**, 13006–13014.
48 M. Choi, K. Na, J. Kim, Y. Sakamoto, O. Terasaki and R. Ryoo, *Nature*, 2009, **461**, 246–249.
49 Z. Guo, G. Xiong, L. Liu, W. Song and Q. Jia, *CrystEngComm*, 2017, **19**, 2695–2701.

 